

# Long-Term Cloud-Resolving Model Simulations of Cloud Properties and Radiative Effects of Cloud Distributions

Xiaoqing Wu and Sunwook Park

Department of Geological and Atmospheric Sciences  
Iowa State University, USA

## Abstract

The year-long cloud-resolving model (CRM) simulation forced with the observed large-scale forcing provides a unique approach to generating the long-term thermodynamic and dynamic consistent cloud properties, documenting the characteristics of cloud horizontal inhomogeneity and vertical overlap, and evaluating their effects on the radiative fluxes and heating rates. In this study, statistical analysis is conducted to evaluate the year-long CRM simulations against available observations. The CRM-produced cloud liquid and ice water paths for overcast and non-precipitating clouds agree with observations in terms of monthly and diurnal cloud occurrence frequency. The vertical distribution of liquid and ice water simulated by CRM is also generally consistent with that from observational estimates. Significant of cloud horizontal inhomogeneity and its radiative effects are quantified by the diagnostic radiation calculation using CRM outputs. The assumption of homogeneous clouds overestimates the total cloud albedo and underestimates the outgoing longwave flux. The redistribution of CRM cloud fraction profile based on three existing overlap assumptions (maximum, minimum, and random) indicates that none of them is able to reproduce the CRM total cloud fraction. The maximum overlap assumption systematically underestimates the total cloud fraction, while the random and minimum overlap assumptions systematically overestimate the total cloud fraction.

Key words: Cloud-resolving model (CRM), cloud and radiative properties, cloud horizontal inhomogeneity and vertical overlap

## 1. Introduction

Representation of cloud-radiation interactions is a major challenge for climate simulations. Since convection and clouds are all subgrid-scale processes, uncertainties in convection and cloud parameterizations further complicate the treatment of subgrid cloud distributions in the radiation parameterization of general circulation models (GCMs). In general, GCMs predict cloud cover fractions and hydrometeor concentrations only in discrete vertical layers where clouds are assumed to be horizontally homogeneous in a coarse grid. They do not explicitly specify vertical geometric associations or horizontal optical variations of clouds. Subsequently, clouds within a GCM grid are represented as a single effective volume by the use of cloud inhomogeneity parameter and vertical overlap assumptions (e.g., Geleyn and Hollingsworth 1979; Stephens 1984; Tian and Curry 1989; Cahalan et al. 1994; Liang and Wang 1997; Oreopoulos and Davies 1998; Barker et al. 1999; Morcrette and Jakob 2000; Li 2000; Fu et al. 2000; Collins 2001; Hogan and Illingworth 2003; Stephens et al. 2004; Liang and Wu 2005; Wu and Liang 2005; Wood et al. 2005; Gu and Liou 2006; Shonk and Hogan 2008). Since complete observations of cloud systems are impossible and available measurements are very limited, quantification of the effects of cloud horizontal inhomogeneity and vertical overlap is difficult.

The development of cloud-resolving models (CRMs) provides a unique opportunity to study this problem. CRM-produced cloud condensate distributions have been used increasingly by the radiation community for various purposes. While GCMs require convection and cloud parameterizations, CRMs explicitly resolve convection and mesoscale organization, where cloud microphysical processes and cloud-radiation interactions directly respond to the cloud-scale dynamics (Grabowski et al. 1996, 1998, 1999; Wu et al. 1998, 1999; Wu and Moncrieff 2001). In particular, fine spatial resolution enables CRMs to depict more realistically the detailed structure of cloud systems, including cloud geometric and radiative properties. Wu and Moncrieff (2001) quantified the radiative effect of subgrid cloud variability using diagnostic calculations of the NCAR Community Climate Model version 3 (CCM3) radiative transfer scheme (Kiehl et al. 1996) and showed important impacts of subgrid cloud variability on both shortwave and longwave radiative fluxes.

Successful long-term CRM simulations of the TOGA COARE (Tropical Ocean Global Atmosphere - Coupled Ocean Atmosphere Response Experiment) cloud systems helped establish the first intercomparison project of CRMs under the GCSS (GEWEX Cloud System Study) (Moncrieff et al. 1997). Uncertainties in the estimation of large-scale forcing and the retrieval of shortwave radiation at the top of the atmosphere (TOA) during TOGA COARE have also been recognized (e.g., Wu et al. 2000). Obviously, a thermodynamically and

dynamically coherent forcing data set and consistent radiative fluxes at the TOA and the surface are needed for CRM simulations and validation. The US Department of Energy (DOE) Atmospheric System Research (ASR) program offers such datasets. The large-scale forcing datasets were constrained by column budgets of dry static energy and moisture using the variational analysis (Zhang and Lin 1997). Recently, year-long (year 2000) CRM simulations were conducted over the central US by Wu et al. (2008) to investigate the seasonal variation of radiative and cloud properties, and by Park and Wu (2010) to examine the effects of prescribed evolving surface albedo on cloud and radiative properties.

In this extended abstract, the cloud horizontal inhomogeneity and vertical overlap and their effects on radiative properties are investigated using the year-long CRM simulations. The Iowa State University (ISU) CRM is briefly described in the next section. The year-long cloud properties simulated by ISUCRM are validated against observations in section 3. The cloud distributions and their impacts on radiative fluxes and radiative heating rates are examined in section 4. A summary is given in section 5.

## 2. ISU cloud-resolving model

The ISUCRM is developed from the Clark-Hall anelastic cloud model (Clark et al. 1996) with modifications to physical processes important for long-term simulations of cloud systems (Grabowski et al. 1996, 1998, 1999; Wu et al. 1998, 1999, 2008; Wu and Moncrieff 2001). Microphysical processes are treated by the Kessler (1969) bulk warm rain parameterization and the Koenig and Murray (1976) bulk ice parameterization. The ice scheme predicts two types of ice particles; type A ice of slowly falling and low-density (unrimed or lightly rimed) particles, and type B ice of fast-falling and high-density graupel. Each type of ice is represented by two variables (i.e., ice water mixing ratio and number concentration). The radiative process is handled by the radiation scheme of the National Center for Atmospheric Research (NCAR) Community Climate Model version 3 (CCM3; Kiehl et al. 1996) with the use of binary liquid and type A ice clouds, which have effective radii of 10 and 30  $\mu\text{m}$ , respectively. The subgrid-scale mixing is parameterized using the first-order eddy diffusion method of Smagorinsky (1963). A nonlocal vertical diffusion scheme (Troen and Mahrt 1986; Holtslag and Moeng 1991; Hong and Pan 1996) is used to distribute the surface latent and sensible heat fluxes within the boundary layer.

## 3. Year-long CRM simulation

The year-long (January 3-December 31, 2000) two-dimensional (2D) CRM simulation is forced by the hourly large-scale forcing data which is constructed using the variational analysis of National Oceanic and Atmospheric Administration rapid update cycle datasets constrained by the surface and top of the atmosphere

(TOA) observations over the Atmospheric Radiation Measurement (ARM) Southern Great Plain (SGP) site including precipitation, latent and sensible heat fluxes and radiative fluxes (Xie et al. 2004). The CRM domain is 600 km in the east-west direction and 40 km in the vertical. The horizontal resolution is 3 km, and the vertical resolution is varied from 100 m near the surface, through 550-850 m between 5 and 12 km, to 1500 m at the model top. The time step is 15 seconds. Periodic lateral boundary conditions, and free-slip bottom and top boundary conditions, are applied with a gravity wave absorber located between 16 km and the model top. The domain-averaged wind is relaxed to the observed wind every time step using a 2-h time scale. The observed evolving surface sensible and latent heat fluxes are applied in the simulation. The surface upward longwave radiative flux is calculated by the observed evolving surface temperature. The surface albedo of direct and diffuse incident solar radiation for two spectral intervals (0.2-0.7 and 0.7-5.0  $\mu\text{m}$ ) is evolved based on observed surface albedo. The radiative fluxes and heating rates are calculated every 300 seconds and applied at intermediate times.

Statistical comparison is made between the year-long CRM simulation and several value added products such as the continuous baseline microphysical retrieval (MICROBASE) cloud liquid and ice water properties and the column physical characterization product (CPC). The CRM-simulated year-long cloud liquid water path is in good agreement (correlation coefficient of 0.73) with the ARM retrievals over SGP. The simulated cloud systems have 50% more ice water than liquid water in annual mean. Figure 1 shows the yearly-averaged profiles of liquid water content (LWC) for each bin of vertical integrated liquid water path (LWP) from the CRM and ARM observations including the column physical characterization product (CPC) and the continuous baseline microphysical retrieval (MICROBASE). There are three groups of LWP: small (1-10  $\text{g m}^{-2}$ ), medium (10-100  $\text{g m}^{-2}$ ), and large (100-1000  $\text{g m}^{-2}$ ) value groups with the bin size of 1, 10 and 100, respectively. In the large LWP group, the peak of LWC from the model exists at around 2 km, while the peak from CPC and MICROBASE occurs around 1.5 km and near the surface, respectively. In the medium group, there are two peaks of LWC at 1 and 2 km from the CRM and observations. In the small LWP group, however, the LWC peak occurs around 1 km from CRM and MICROBASE, while there is a large peak around 6 km in CPC. This feature is an artifact of the CPC retrieval scheme at very low LWP values and should be neglected. The CRM-produced LWC fields are in reasonable agreement with the observations in the large and medium LWP groups. In the small LWP group, however, three products are different from each other. It is probably caused by the fact that small ice crystals above or in the melting level are detected as liquid water in their retrieval algorithm.

Similar comparison between the CRM and observations is shown in Fig. 2 for the ice water content

(IWC). The peaks of IWC are around 7, 5.5 to 4.5 km for small, medium and large IWP groups, respectively. These suggest that large IWP clouds tend to exist at lower levels, while small IWP clouds are likely to occur at higher levels. It is noted that the CRM has a near surface peak of IWC in the small IWP group that does not appear in the observations. Over ARM SGP, there are often supercooled stratus clouds; temperatures are in the 260 K range but these clouds are generally liquid and produce liquid drizzle. The CRM may be producing light frozen drizzle from these clouds and then dropping the particles to the surface as frozen precipitation.

Figure 3 presents the frequency histograms of daytime (i.e., 8-16 LST) cloud optical depth from the CRM and multifilter rotating shadowband radiometer (MFRSR) for four seasons. In spring and winter, the distributions of the CRM and MFRSR are very similar to each other. However, in summer and fall, the large values of cloud optical depth from the MFRSR are greater than those from the CRM. Overall, the general frequency distributions of cloud optical depth from the CRM and MFRSR have a good agreement.

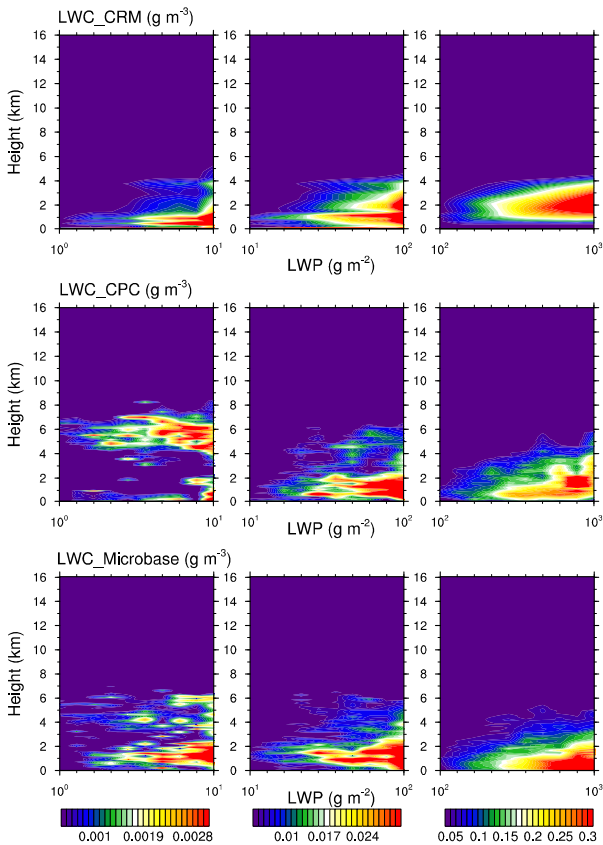


**Figure 1.** Yearly-averaged profiles of LWC for each bin of vertically-integrated LWP from the CRM, CPC, and MICROBASE. The bin sizes are 1, 10, and 100  $\text{g m}^{-2}$  for three categories (i.e., small size of 1-10  $\text{g m}^{-2}$ , medium size of 10-100  $\text{g m}^{-2}$ , and large size of 100-1000  $\text{g m}^{-2}$ ) of LWP, respectively.

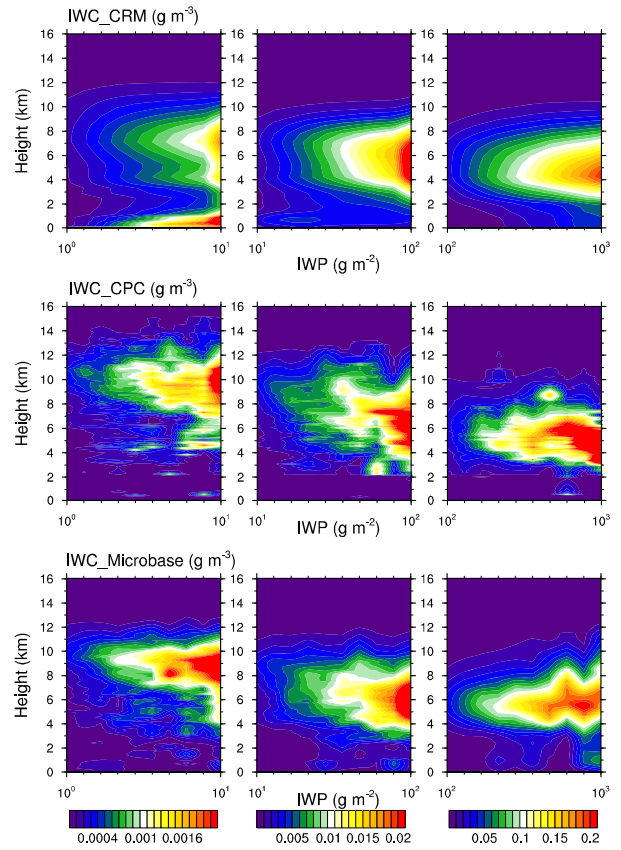


**Figure 2.** Yearly-averaged profiles of IWC for each bin of vertically-integrated ice water path (IWP) from the CRM, CPC, and MICROBASE. The bin sizes are 1, 10, and 100  $\text{g m}^{-2}$  for three categories (i.e., small size of 1-10  $\text{g m}^{-2}$ , medium size of 10-100  $\text{g m}^{-2}$ , and large size of 100-1000  $\text{g m}^{-2}$ ) of IWP, respectively.

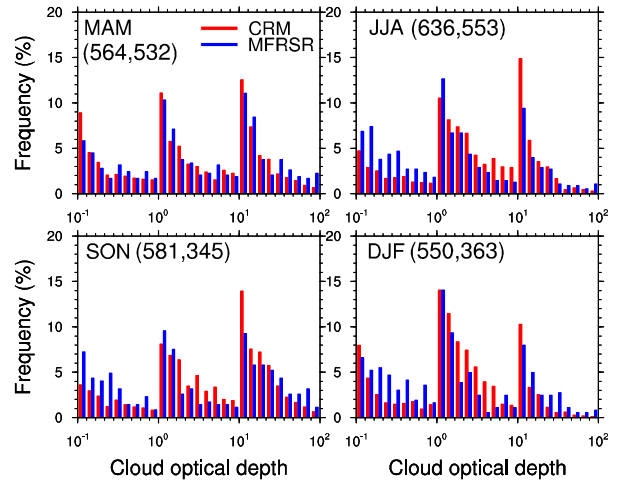


**Figure 3.** Frequency histograms of daytime cloud optical depth from the CRM and MFRSR for four seasons based on hourly mean values. The bin sizes are 0.1, 1, and 10 for three categories (i.e., small size of 0.1-1, medium size of 1-10, and large size of 10-100), respectively. The first and second numbers in the parentheses indicate samples from the CRM and MFRSR, respectively.

#### 4. Cloud horizontal and vertical distribution

To quantify the cloud horizontal inhomogeneity in the CRM, we adopt the inhomogeneity parameter  $\chi$ , first introduced by Cahalan et al. (1994). The parameter is defined as the ratio of the logarithmic and linear average of a cloud optical depth distribution:

$$\chi = \frac{e^{\overline{\ln \tau}}}{\overline{\tau}}, \quad 0 < \chi < 1,$$

where  $\overline{\tau} = \int \tau p(\tau) d\tau$  and  $\overline{\ln \tau} = \int \ln \tau p(\tau) d\tau$ .

$p(\tau)$  is the probability distribution function of cloud optical depth  $\tau$ . If  $\chi$  is close to 0 the clouds are horizontally more inhomogeneous, while the value close to 1 indicates more homogeneous clouds. The cloud optical depth is calculated from liquid water path (LWP) and ice water path (IWP) using the same method done by Wu et al. (2008). The cloud inhomogeneity parameters are calculated inside clouds at every 15-min time step. Seasonal frequency distributions of the inhomogeneity parameters are showed in Fig. 4. The clouds in spring are slightly more inhomogeneous with a mean  $\chi$  of 0.44. The largest bin is 0.2-0.25 with about 9% of frequency. In summer, the CRM-produced clouds are much more inhomogeneous with 0.37 of mean value. The occurrence frequency is about 40% for the clouds whose values of inhomogeneity parameter are in 0.1-0.3. Only about 6% of frequency is occupied by relatively homogeneous clouds with the values greater than 0.8. The inhomogeneous and homogeneous clouds almost equivalently occur in fall. However, the clouds in winter usually are homogeneous; the mean value of the parameter is 0.71. Over 40% of the clouds have the parameter values greater than 0.8. Only few inhomogeneous clouds occur in winter.

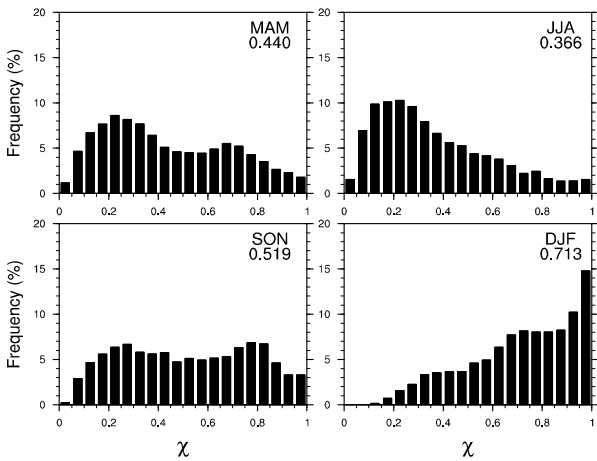


**Figure 4.** Seasonal variation of frequency histograms for cloud inhomogeneity parameters ( $\chi$ ). The numbers for each season indicate mean values of the parameter.

To examine the cloud vertical overlap and its effects on radiative properties, three overlap assumptions

(i.e., the maximum, minimum and random overlap assumptions) (Tian and Curry 1989) are analyzed,

$$TC_{max} = \text{Max}(A_1, A_2, \dots, A_n)$$

$$TC_{min} = \text{Min}\left(\sum_{i=1}^n A_i, 1\right)$$

$$TC_{ran} = 1 - (1 - A_1)(1 - A_2) \dots (1 - A_n)$$

where  $A_1, A_2, \dots, A_n$  are the cloud fraction for each level and TC is the total cloud fraction from three assumptions (max, min and ran). Figure 5 shows the seasonal scatter diagrams of total cloud fractions from the CRM and three overlap assumptions based on daily mean values. The total cloud fractions from the CRM are obtained by actual fractional coverage of the cloudy boxes in the CRM domain. The minimum overlap assumption usually much overestimates the cloud fraction during the four seasons. The discrepancies from the CRM values are 0.25, 0.22, 0.14 and 0.12 for spring, summer, fall and winter, respectively. However, the maximum overlap assumption systematically underestimates the cloud fraction for the four seasons. The total cloud fractions are smaller about 0.08, 0.10, 0.22 and 0.04 for each season compared to the CRM values. The random overlap assumption also tends to produce greater cloud fractions than the CRM through the four seasons, but smaller compared to the minimum overlap assumption. The cloud fractions from the random overlap assumption are larger compared to the CRM about 0.19, 0.16, 0.10 and 0.09 for spring, summer, fall and winter, respectively. Thus, the minimum and random overlap assumptions overestimate the total cloud fractions about 0.18 and 0.13, respectively, greater than the CRM, while the maximum overlap assumption underestimates about 0.08 smaller compared to the CRM in the annual mean. The CRM-simulated clouds are usually located between the maximum and random overlaps, and the winter clouds from the CRM are more maximally overlapped.

## 5. Summary

The analysis of Cahalan's inhomogeneity parameter using the year-long CRM simulation demonstrates seasonally varied cloud inhomogeneity with more inhomogeneous clouds in summer but more homogeneous clouds in winter. It is evident that the within-cloud variance must be incorporated for determining inhomogeneous corrections to plane-parallel cloud albedo and cloud emissivity estimates in GCMs. The maximum, minimum and random vertical overlap assumptions cannot properly represent the CRM cloud overlaps. Large biases show in the total cloud fractions, radiative fluxes at the surface and TOA, and the radiative heating rates. It suggests that the physically based vertical overlap which treats characteristic structure differences between major cloud types (e.g., convective, anvil and stratiform) is needed to incorporate the cloud

geometric association and optical inhomogeneity effects in the radiation calculation.

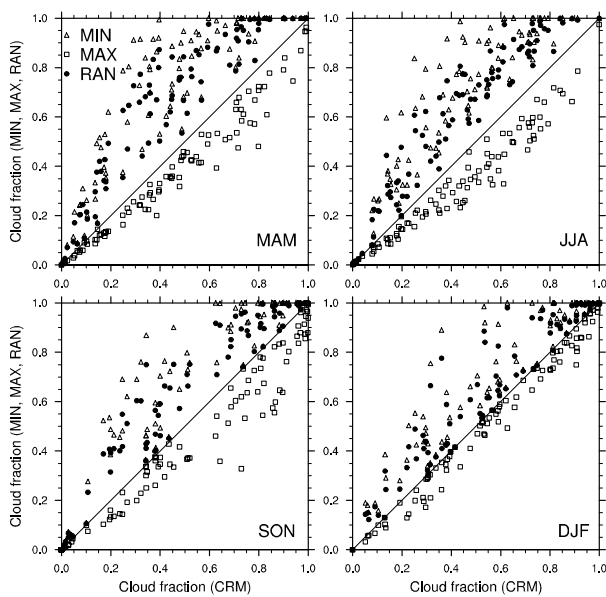


**Figure 5.** Scatter diagrams of total cloud fraction from the CRM versus that derived from each overlap assumption (minimum, maximum and random) based on daily mean for the four seasons.

## References

- Barker, H. W., G. L. Stephens, and Q. Fu, 1999: The sensitivity of domain-averaged solar fluxes to assumptions about cloud geometry. *Quart. J. Roy. Meteor. Soc.*, **125**, 2127-2152.
- Cahalan, R. F., W. Ridgway, W. J. Wiscombe, T. L. Bell, and J. B. Snider, 1994: The albedo of fractal stratocumulus clouds. *J. Atmos. Sci.*, **51**, 2434-2455.
- Clark, T. L., W. D. Hall, and J. L. Coen, 1996: Source code documentation for the Clark-Hall cloud-scale model: Code version G3CH01. *NCAR Tech. Note*, NCAR/TN-426+STR, 137 pp.
- Collins, W. D., 2001: Parameterization of generalized cloud overlap for radiative calculations in general circulation models. *J. Atmos. Sci.*, **58**, 3224-3242.
- Fu, Q., M.C. Cribb, H.W. Barker, S.K. Krueger, and A. Grossman, 2000: Cloud geometry effects on atmospheric solar absorption. *J. Atmos. Sci.*, **57**, 1156-1168.
- Geleyn, J. F., and A. Hollingsworth, 1979: An economical analytical method for the computation of the interaction between scattering and line absorption of radiation. *Contrib. Atmos. Phys.*, **52**, 1-16.
- Grabowski, W. W., X. Wu, and M. W. Moncrieff, 1996: Cloud resolving modeling of tropical cloud systems during Phase III of GATE. Part I: Two-dimensional experiments. *J. Atmos. Sci.*, **53**, 3684-3709.
- Grabowski, W.W., X. Wu, M.W. Moncrieff, and W.D. Hall, 1998: Cloud resolving modeling of tropical cloud systems during Phase III of GATE. Part II: Effects of resolution and the third spatial dimension. *J. Atmos. Sci.*, **55**, 3264-3282.
- Grabowski, W.W., X. Wu, and M.W. Moncrieff, 1999: Cloud resolving modeling of tropical cloud systems during Phase III of GATE. Part III: Effects of cloud microphysics. *J. Atmos. Sci.*, **56**, 2384-2402.
- Gu, Y., and K. N. Liou, 2006: Cirrus cloud horizontal and vertical inhomogeneity effects in a GCM. *Meteorol. Atmos. Phys.*, **91**, 223-235.
- Hogan, R. J., and A. J. Illingworth, 2003: Parameterizing ice cloud inhomogeneity and the overlap of inhomogeneities using cloud radar data. *J. Atmos. Sci.*, **60**, 756-767.
- Holtlag, A. A. M., and C.-H. Moeng, 1991: Eddy diffusivity and countergradient transport in the convective atmospheric boundary layer. *J. Atmos. Sci.*, **48**, 1690-1698.
- Hong, S.-Y., and H.-L. Pan, 1996: Nonlocal boundary layer vertical diffusion in a medium-range forecast model. *Mon. Wea. Rev.*, **124**, 2322-2339.
- Kessler, E., 1969: On the distribution and continuity of water substance in atmospheric circulations. *Met. Monog.*, **32**, 84 pp.
- Kiehl, J. T., J. J. Hack, G. B. Bonan, B. A. Boville, B. P. Briegleb, D. L. Williamson, and P. J. Rasch, 1996: Description of the NCAR Community Climate Model (CCM3). *NCAR Tech. Note*, NCAR/TN420+STR, 152 pp.
- Koenig, L. R., and F. W. Murray, 1976: Ice-bearing cumulus cloud evolution: Numerical simulation and general comparison against observations. *J. Appl. Meteorol.*, **15**, 747-762.
- Li, J., 2000: Accounting for overlap of fractional cloud in infrared radiation. *Q. J. R. Meteorol. Soc.*, **126**, 3325-3342.
- Liang, X.-Z., and W.-C. Wang, 1997: Cloud overlap effect on general circulation model climate simulations. *J. Geophys. Res.*, **102**, 11039-11047.
- Liang, X.-Z., and X. Wu, 2005: Evaluation of a GCM subgrid cloud-radiation interaction parameterization using cloud-resolving model simulations. *Geophys. Res. Lett.*, **32**, L06801, doi:10.1029/2004GL022301.
- Morcrette, J. J., and C. Jakob, 2000: The response of the ECMWF model to changes in the cloud overlap assumption. *Mon. Wea. Rev.*, **128**, 1707-1732.
- Oreopoulos, L., and R. Davies, 1998: Plane parallel albedo biases from satellite observations. Part II: Parameterizations for bias removal. *J. Climate*, **11**, 933-944.
- Park, S., and X. Wu, 2010: Effects of surface albedo on cloud and radiation processes in cloud-resolving model simulations. *J. Atmos. Sci.*, in press.
- Shonk, J. K. P., and R. J. Hogan, 2008: Tripleclouds: An efficient method for representing horizontal cloud inhomogeneity in 1D radiation schemes by using three regions at each height. *J. Climate*, **21**, 2352-2370.
- Smagorinsky, J., 1963: General circulation experiments with the primitive equations. I. The basic experiment. *Mon. Wea. Rev.*, **91**, 99-164.

- Stephens, G. L., 1984: The parameterization of radiation for numerical weather prediction and climate models. *Mon. Wea. Rev.*, **112**, 826-867.
- Tian, L., and J. A. Curry, 1989: Cloud overlap statistics. *J. Geophys. Res.*, **94**, 9925-9935.
- Troen, I., and L. Mahrt, 1986: A simple model of the atmospheric boundary layer: Sensitivity to surface evaporation. *Bound.-Layer Meteor.*, **37**, 129-148.
- Wood, N. B., P. M. Gabriel, and G. L. Stephens, 2005: An assessment of the parameterization of subgrid-scale cloud effects on radiative transfer. Part II: Horizontal inhomogeneity. *J. Atmos. Sci.*, **62**, 2895-2909.
- Wu, X., M.W. Moncrieff, and K.A. Emanuel, 2000: Evaluation of large-scale forcing during TOGA COARE for cloud-resolving models and single-column models. *J. Atmos. Sci.*, **57**, 2977-2985.
- Wu, X., and M. W. Moncrieff, 2001: Long-term behavior of cloud systems in TOGA COARE and their interactions with radiative and surface processes. Part III: Effects on the energy budget and SST. *J. Atmos. Sci.*, **58**, 1155-1168.
- Wu, X., and X.-Z. Liang, 2005: Effect of subgrid cloud-radiation interaction on climate simulations. *Geophys. Res. Lett.*, **32**, L24806, doi:10.1029/2005GL024432.
- Wu, X., W. W. Grabowski, and M. W. Moncrieff, 1998: Long-term behavior of cloud systems in TOGA COARE and their interactions with radiative and surface processes. Part I: Two-dimensional Modeling Study. *J. Atmos. Sci.*, **55**, 2693-2714.
- Wu, X., W. D. Hall, W. W. Grabowski, M. W. Moncrieff, W. D. Collins, and J. T. Kiehl, 1999: Long-term behavior of cloud systems in TOGA COARE and their interactions with radiative and surface processes. Part II: Effects of ice microphysics on cloud-radiation interaction. *J. Atmos. Sci.*, **56**, 3177-3195.
- Wu, X., S. Park, and Q. Min, 2008: Seasonal variation of cloud systems over ARM SGP. *J. Atmos. Sci.*, **65**, 2107-2129.